

An embedded cohesive crack model for finite element analysis of brickwork masonry fracture

E. Reyes , J.C. Gálvez , M.J. Casati , D.A. Cendón , J.M. Sancho , J. Planas

Universidad Politécnica de Madrid, E.T.S. Ingenieros de Caminos, Canales y Puertos, Dep. Ingeniería Civil: Construcción, C/ Profesor Aranguren s/n, 28040 Madrid, Spain

Universidad Politécnica de Madrid, E.U. Ingeniería Técnica Aeronáutica, Dep. Vehículos Aeroespaciales., Pza. Cardenal Cisneros s/n, 28040 Madrid, Spain

Universidad Politécnica de Madrid, E.T.S. Ingenieros de Caminos, Canales y Puertos, Dep. Ciencia de Materiales, C/ Profesor Aranguren s/n, 28040 Madrid, Spain

Universidad CEU San Pablo, Escuela Politécnica Superior, Campus Montepríncipe, Boadilla del Monte, 28668 Madrid, Spain

A B S T R A C T

This paper presents a numerical procedure for fracture of brickwork masonry based on the strong discontinuity approach. The model is an extension of the cohesive model prepared by the authors for concrete, and takes into account the anisotropy of the material. A simple central-force model is used for the stress versus crack opening curve. The additional degrees of freedom defining the crack opening are determined at the crack level, thus avoiding the need of performing a static condensation at the element level. The need for a tracking algorithm is avoided by using a consistent procedure for the selection of the separated nodes. Such a model is then implemented into a commercial code by means of a user subroutine, consequently being contrasted with experimental results. Fracture properties of masonry are independently measured for two directions on the composed masonry, and then input in the numerical model. This numerical procedure accurately predicts the experimental mixed-mode fracture records for different orientations of the brick layers on masonry panels.

Keywords:

Masonry

Mixed-mode fracture

Finite element analysis

Embedded crack

Strong discontinuity approach

Cohesive model

1. Introduction

Masonry is a building material profusely used for façades and internal walls in buildings. A frequent problem of brickwork masonry structural elements and walls is cracking, associated with differential settlements and/or excessive deflections of slabs throughout the life of the structure [1,2]. Cracking of masonry is caused by the fragility and low capacity of the masonry, when accompanying structural elements such as floors, beams or foundations, in their movements. This problem is usually one of fracturing, where the wall is cracked under mixed-mode fracture under quasi-static loading.

Until now, the study of brick masonry failure has been focussed on compression [3–6], compression/shear failure mechanisms [7–15] and out of plane bending [16–18]. A certain effort has been given to studying tensile failure and in plane flexural/tensile mechanisms of brickwork masonry (mode I fracture) [19–23], and less time (based on the fracture mechanics approach), to tensile/shear failure [24–28]. Such a tensile/shear failure is known as mixed-mode fracture (combination of the modes I and II).

Masonry may be considered a composite material made of brick units and mortar arranged forming layers, namely bed joints. The interface between brick and mortar is usually the weakest part of the masonry [7,29]. Depending on the scale, the

Nomenclature

a	finite element node index
A	finite element area
$b_a(\mathbf{x})$	shape function gradient for node a
\mathbf{E}	elastic moduli tensor
$f(w)$	classical softening function for mode I
f_t	tensile strength
f_{t1}	tensile strength in the bed joints direction
f_{t2}	tensile strength in the head joints direction
G_F	specific fracture energy
h	triangular element height
$H(\mathbf{x})$	Heaviside jump function
L	crack length in the finite element
\mathbf{n}	normal vector
$N_a(\mathbf{x})$	traditional shape function for node a
\mathbf{t}	traction vector
\mathbf{u}_a	nodal displacement
w	crack opening
\mathbf{w}	crack displacement vector
\hat{w}	equivalent crack opening
α	angle between the bed joints direction and the OX axis
β	angle between the first principal stress direction and the OX axis
γ	angle between the crack direction and the bed joints direction
$\boldsymbol{\varepsilon}^c$	continuous part of the strain tensor
$\boldsymbol{\varepsilon}^a$	apparent part of the strain tensor
$\boldsymbol{\sigma}$	stress vector, with components $(\sigma_x, \sigma_y, \tau_{xy})$
θ	angle between first principal stress direction and bed joints direction in the masonry
σ_1	first principal stress
σ_γ	normal stress to the arbitrary direction (which forms an angle γ with bed joints)
1	direction of the bed joints of masonry
2	direction of the head joints of masonry
I	first principal stress direction
II	second principal stress direction

Abbreviations

CMOD	crack mouth opening displacement
EAS	enhanced assumed strain method
FE	finite element
FEM	finite element method
SDA	strong discontinuity approach
TPB	three point bending

modelling of the masonry can be performed with different levels of abstraction, from a detailed representation of bricks, mortar and joints [7,30] to a global analysis as an isotropic or anisotropic continuum [29,31–33]. The grade of refinement is directly related with the problem being analysed.

A micro-modelling approach [22,33–35] is useful for detailed analysis of the masonry failures on a small size structural element. Bricks, mortar and interfaces between mortar and brick are separately represented. The non-linear behaviour of the interfaces has been studied in detail by means of such models [36,37], as well as the individual fracture of mortar and bricks [22]. However, the failure analysis of large and geometrically complex structures using these models is usually unfeasible. The modelisation of the structure is highly time consuming, in addition to some of the parameters of the material needed for computation being quite difficult to measure in real (especially ancient) buildings. Homogenisation techniques [10,34,38–42] are extremely useful in the numerical analysis of these problems and reduce the computational cost, though certain practical difficulties do remain.

A meso-modelling approach represents a complementary way to model the masonry fracture [8,14,24,27,42–44]. Such an approach is promising for large masonry structures, in which detailed modelling of brick and mortar leads to an expensive and unfeasible analysis. This paper presents a meso-mechanical procedure for the analysis of mixed-mode fracture of brick masonry based on the cohesive crack model embedded in a finite element. Focussed on the material, the model does not make any distinction between masonry units (bricks), mortar and joints, averaging the effect of the composite material through the formulation of a fictitious continuous material. The material is assumed to be homogeneous and anisotropic.

The embedded cohesive crack model has been successfully used for mixed-mode fracture of concrete and mortar [45–47,53], which are considered homogenous and isotropic materials at meso-level approach. In this work the model is extended to anisotropic materials, like brick masonry.

The SDA [48] has successfully completed the two main conventional approaches, based on the FEM, to fracture of concrete and quasi-brittle materials: the smeared crack and the discrete crack. In contrast to the smeared crack model, in SDA the fracture zone is represented as a discontinuous displacement surface. In comparison with the discrete crack approach, in SDA the crack geometry is not restricted to the inter-element lines, as the displacement jumps are embedded in the corresponding finite element displacement field. A comparative review of the various approaches to the embedded crack concept is presented by Jirásek [49].

Embedding discontinuous displacements in the element formulation is not the only way to implement the SDA in the FEM. Recently, the so-called *extended finite element method*, based on nodal enrichment and the partition of unity concept, has opened a very fruitful way to the modelling of fracture. However, extended finite elements require a greater implementation effort compared to elements with embedded discontinuities. The advantages and disadvantages of both strategies can be found in [50].

The SDA provides a consistent framework to transform a weak discontinuity, in which the displacement is continuous though the strain is discontinuous at the boundaries of a band of a certain width h , into a strong discontinuity in which displacement is discontinuous at a surface. Thus, the strong discontinuity (displacement jump) is obtained as the limit of a weak discontinuity band when the bandwidth h tends to zero. Hence, the discrete constitutive model for the discontinuity naturally arises, induced by the continuum model. This is an elegant and sound standpoint for the study of shear bands in soils and metals. However, in the fracture of quasi-brittle materials it is simpler and more effective to use a discrete constitutive model that relates the tractions and displacement jumps at the discontinuity line. This approach is used in this study.

A consistent derivation of the finite element with embedded discontinuities can be performed in the frame of the EAS proposed by Simo and Rifai [51]. The strain induced for the displacement jumps are then tackled as additional incompatible modes. A problem of this approach is that, as the additional modes are determined at the element level, the progress of the crack may be locked because of kinematical incompatibility among the cracks in neighbouring elements.

One solution to avoid this problem is to use an algorithm to re-establish the geometric continuity of the crack line across the elements, a procedure known as *crack tracking* [52]. Most practical implementations use tracking to avoid crack locking. Moreover, some implementations further require establishing exclusion zones defined to avoid the formation of new cracks in the vicinity of existing cracks. These kinds of algorithms cause inconvenience in the implementation of the embedded crack elements in standard finite element programs, and are therefore of greater interest in developing a method that circumvents the need of the crack path enforcement.

This work presents a procedure, based on SDA, which reproduces the fracture process of brick masonry under mixed loading using the cohesive crack approach. The paper seeks to show, by means of simple considerations, how using finite elements with an embedded cohesive crack is an efficient option to model the mixed-mode fracture of a complex material like masonry. In contrast with previous works [45–48,50,51] the model takes into account the anisotropy of the masonry, and it does not require crack tracking or establishing exclusion zones to avoid crack locking.

With this model as a framework, fracture properties of the entire masonry are independently determined for at least two main directions of masonry by specific tests performed on this material, then being input to numerical simulation, where masonry is treated as a homogeneous material. The result is an anisotropic cohesive fracture model, which can predict the behaviour of the whole masonry without resort to any kind of fitting or tuning procedure.

To check the model, a series of mixed fracture tests, previously developed [26,27], on small masonry panels under TPB with non-symmetric loading were selected. As it will be shown later, the model can accurately predict loads and displacement throughout the test records. Tests of masonry panels with different orientations of the bed joints were performed.

The adopted experimental work is not intended to be either a small-scale testing or modelling of real masonry walls. With this paper, the authors seek to emphasise that with this new approach, based on the embedded cohesive crack modelling applied to masonry, it is possible to analyse the mixed-mode fracture behaviour of this complex material. It is acknowledged that further work must be carried out to extend this modelling to full-scale masonry structures.

Whereas the following section examines the cohesive crack model, Section 3 studies finite element modelling. Numerical implementation of the model is presented in Section 4. Overview of the selected mixed-mode fracture tests is then presented and discussed in Section 5, with the numerical analysis of these tests being presented in Section 6. Discussion is presented in Section 7. Finally, the conclusions obtained from the model and the experiments are presented in Section 8.

2. The cohesive crack model

As mentioned above, the meso-scale approach is adopted in this work. Such an approach does not make any distinction between masonry bricks, mortar and joints, averaging the effect of the composite material through the formulation of a fictitious continuous material. This material is homogeneous, anisotropic and shows cohesive behaviour under tensile cracking.

2.1. Overview of the cohesive crack model for isotropic materials

The cohesive crack model is generally accepted as a realistic simplification of the fracture of quasi-brittle materials. Such a model was proposed by Hillerborg et al. [53] in the late seventies, based on the pioneering works of Dugdale [54] and

Barenblatt [55], and has been successful in the analysis of the fracture of concrete and concrete-like materials since its proposal, as shown in Ref. [56]. The softening function, $\sigma = f(w)$, is the main ingredient of the cohesive crack model. This function, a material property, relates the stress σ acting across the crack faces to the corresponding crack opening w (see Fig. 1). In mode I opening, the stress transferred, σ , is normal to the crack faces. A detailed study of this model has been published by Bažant and Planas [57].

Previous works [56,58] have shown that for most experiments described in the literature, cohesive crack growth takes place under predominantly local mode I, which implies that the overall behaviour is dominated by mode I parameters. Therefore, a simple generalisation of the cohesive crack to mixed mode is used which assumes that the traction vector \mathbf{t} transmitted across the crack faces is parallel to the crack displacement vector \mathbf{w} (central-forces model). For monotonic loading in which the magnitude of the crack opening vector $|\mathbf{w}|$ is never decreasing, the relationship reads [45–47]:

$$\mathbf{t} = f(|\mathbf{w}|) \frac{\mathbf{w}}{|\mathbf{w}|} \quad (1)$$

where $f(|\mathbf{w}|)$ is the classical softening function for pure opening mode (Fig. 2). To cope with the possibility of unloading, it is further assumed that the cohesive crack unloads to the origin (Fig. 2) and Eq. (1) is rewritten as:

$$\mathbf{t} = \frac{f(|\tilde{w}|)}{\tilde{w}} \mathbf{w} \quad \text{with } \tilde{w} = \max(|\mathbf{w}|) \quad (2)$$

where \tilde{w} is an equivalent crack opening defined as the historical maximum of the magnitude of the crack displacement vector.

2.2. Cohesive crack model for masonry

The cohesive crack model has been satisfactorily applied to bricks [59] and brickwork masonry [22,24,27]. Nevertheless, on isotropic materials the cohesive crack initiates at the point where the maximum principal stress σ_1 first reaches the

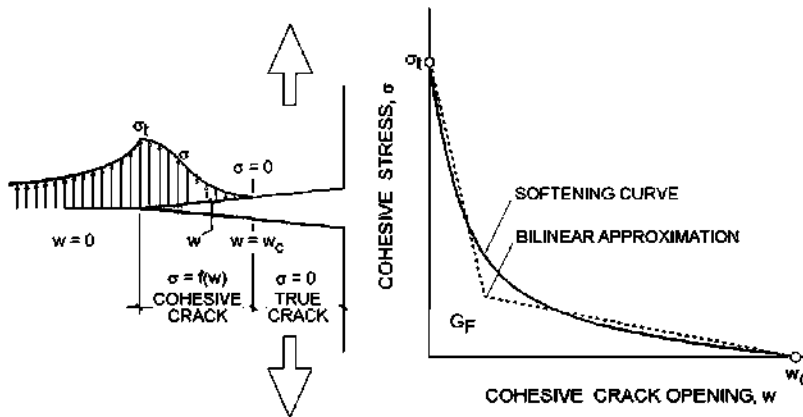


Fig. 1. Cohesive crack, softening function and notation for mode I fracture of cohesive materials.

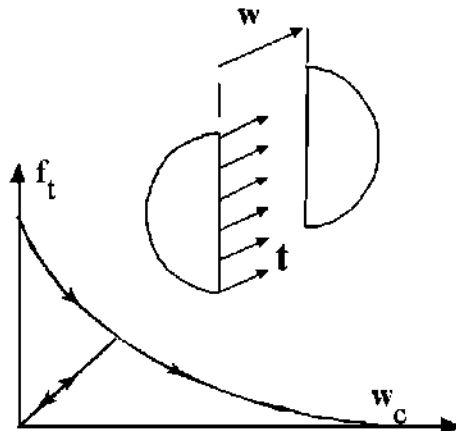


Fig. 2. Sketch of the softening curve, with unloading branch, and central-forces model for the cohesive crack model.

tensile strength f_t , and the crack grows in a normal direction to that of the maximum principal stress. Then, the crack grows predominantly under local mode I. This approach is not valid for anisotropic cohesive materials, such as brick masonry, where the cracking initiation and growth cannot be exclusively expressed in terms of principal stresses, and a failure criterion is also needed. There is large experimental evidence about the dependence of the crack path orientation in brick masonry with the direction of the bed joints [29].

Rankine criterion has been successfully used as a cracking criterion for quasi-brittle materials. In this work a generalised Rankine criterion has been adopted. This criterion balances accuracy and simplicity, especially from the point of view of the experimental determination of the mechanical parameters of the brick masonry.

Fig. 3 shows a panel of brickwork masonry. Axis **1** and axis **2** show the direction of the bed and head joints of the masonry, respectively. OX and OY are the axes of reference in a numerical simulation. **I** and **II** show the principal stress directions. α is the angle between OX axis and **1** direction. β is the angle between OX axis and **I** direction. θ angle measures the rotation between principal stress axis with respect to the principal material axes, and is the addition of the angles α and β .

The direction at which the crack initiates, given by the angle γ relative to **1** direction, is unknown. Such a direction is one that the tensile stress reaches the tensile strength. It is worth noting that whereas in an isotropic material the direction when the crack initiates is given by the maximum principal stress, in anisotropic material there could be another direction in which the tensile stress reaches the strength of the material.

To complete the generalised Rankine criterion it would be of interest to measure the tensile strength of the masonry in different directions, which is quite difficult to carry out in practice. For the sake of simplicity, in this work the material is characterised in two representative directions; for example in their principal directions, and then a function of angle γ is adopted to evaluate the strength in the intermediate directions. To avoid possible convergence problems caused by kink points a sinusoidal curve has been adopted (see Fig. 4). So, the tensile strength is expressed as:

$$f_t(\gamma) = \frac{f_{t1} + f_{t2}}{2} + \frac{f_{t1} - f_{t2}}{2} \cos(2\gamma) \quad (3)$$

Due to the symmetry of the brickwork masonry, this function is symmetrical with respect to axis **1**, and has a period of π .

In accordance with Eq. (2), the tensile strength $f_t(\gamma)$ evolves with the softening parameter \hat{w} , from the initial tensile strength until zero, when the masonry is completely broken. The difference with isotropic material is the dependence of the tensile strength with angle γ .

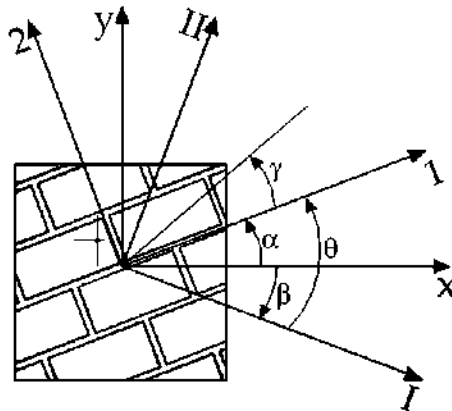


Fig. 3. Sketch of a masonry panel with the directions of the bed and head joints (**1** and **2**), axes of reference (OX and OY) and principal stresses (**I** and **II**).

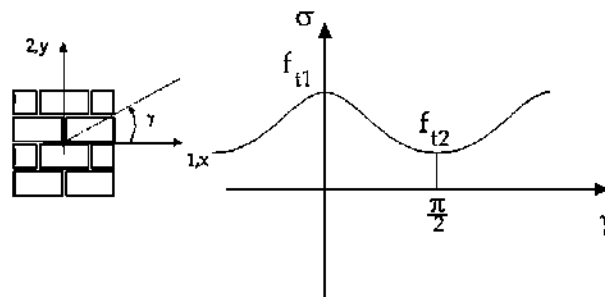


Fig. 4. Graphical representation of the sinusoidal curve for the variation of the tensile strength with γ angle.

The stress state at any point of the masonry, in a 2D analysis, is given by the stress tensor $\boldsymbol{\sigma}$. The normal stress to an arbitrary direction, which forms an angle γ with the bed joints, may be expressed as:

$$\sigma_\gamma = (\boldsymbol{\sigma} \cdot \vec{u}_\gamma)_n = \frac{\sigma_x + \sigma_y}{2} + \frac{\sigma_x - \sigma_y}{2} \cos(2(\gamma + \alpha)) - \tau_{xy} \sin(2(\gamma + \alpha)) \quad (4)$$

The crack initiates (or grows) in this direction (angle γ with bed joints) if σ_γ reaches the actual tensile strength in the normal direction to this one, expressed as:

$$\sigma_\gamma = f_t(\gamma) \quad (5)$$

Eq. (5) is a necessary condition, though inadequate given that these two curves, σ_γ and $f_t(\gamma)$, must intersect in one point. Consequently, as they also have to be tangent at this point, the following additional condition is imposed:

$$\frac{d\sigma_\gamma}{d\gamma} = \frac{df_t(\gamma)}{d\gamma} \quad (6)$$

3. Finite element modelling

This section provides the modelling to describe the masonry cracking in 2D. For this purpose the crack is numerically implemented as a discontinuity embedded in a classical FE. The modelling is mainly based on the authors' proposal for concrete [45–47].

3.1. Overview of the FE formulation

Let be an arbitrary classical finite element defined by a node layout as shown in Fig. 5a. Assume that a straight crack is embedded in it. Take one of the faces of the crack as the reference and its normal \mathbf{n} pointing towards the other face as the positive normal. Let \mathbf{w} be the displacement jump across the crack of the opposite side of the crack with respect to the reference side (see Fig. 5b). The crack splits the element in two sub-domains A^+ and A^- . Following the SDA (e.g., [60]), the approximated displacement field within the element can be written as:

$$\mathbf{u}(\mathbf{x}) = \sum_{a \in A} N_a(\mathbf{x}) \mathbf{u}_a + [H(\mathbf{x}) - N^+(\mathbf{x})] \mathbf{w} \quad (7)$$

where a is the element node index, $N_a(\mathbf{x})$ the traditional shape function for node a , \mathbf{u}_a the corresponding nodal displacement, $H(\mathbf{x})$ the Heaviside jump function across the crack plane (i.e., $H(\mathbf{x}) = 0$ for $\mathbf{x} \in A^-$, $H(\mathbf{x}) = 1$ for $\mathbf{x} \in A^+$), and $N^+(\mathbf{x}) = \sum_{a \in A^+} N_a(\mathbf{x})$.

The strain tensor is obtained from the displacement field as a continuous part $\boldsymbol{\varepsilon}^c$ plus a Dirac's δ function on the crack line. The continuous part, which determines the stress field on the element on both sides of the crack, is given by

$$\boldsymbol{\varepsilon}^c(\mathbf{x}) = \boldsymbol{\varepsilon}^a(\mathbf{x}) - [\mathbf{b}^+(\mathbf{x}) \otimes \mathbf{w}]^s \quad (8)$$

where $\boldsymbol{\varepsilon}^a$ and \mathbf{b}^+ are given by

$$\boldsymbol{\varepsilon}^a(\mathbf{x}) = \sum_{a \in A} [\mathbf{b}_a(\mathbf{x}) \otimes \mathbf{u}_a]^s \quad (9)$$

$$\mathbf{b}^+(\mathbf{x}) = \sum_{a \in A^+} \mathbf{b}_a(\mathbf{x}) \quad (10)$$

with $\mathbf{b}_a(\mathbf{x}) = \text{grad } N_a(\mathbf{x})$ and superscript s indicating a symmetric part of a tensor. Obviously, $\boldsymbol{\varepsilon}^a$ is the *apparent* strain tensor of the element computed from the nodal displacements.

3.2. Crack tractions

Along the cohesive crack line, the jump vector \mathbf{w} and the traction vector \mathbf{t} are to be related by Eq. (2) and the considerations expressed by Eq. (5). For the exact solution, the traction vector is computed locally as $\mathbf{t} = \boldsymbol{\sigma} \cdot \mathbf{n}$. For the finite

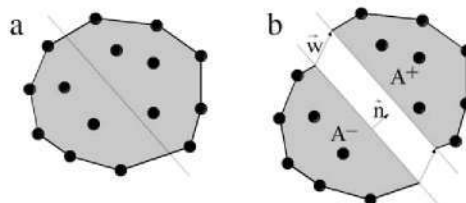


Fig. 5. Finite element with a crack with uniform opening: (a) generic element with nodes and crack line and (b) displacement jump across the crack line.

element, however, we must deal with **approximate tractions and crack jump vectors**, and there is not a single way to determine the relationship between the approximate stress field and the tractions. To simplify the reasoning, we approximate the traction field along the crack line by a constant traction $\bar{\mathbf{t}}$. The determination of $\bar{\mathbf{t}}$ is approximate, and can be carried out in two different ways: (1) as an average along the crack line of the local traction vector $\boldsymbol{\sigma} \cdot \mathbf{n}$, or (2) by forcing the global equilibrium of either A^+ or A^- (which is equivalent, in this case, to using the principle of virtual work). The corresponding equations read:

$$\bar{\mathbf{t}} = \frac{1}{L} \int_L \boldsymbol{\sigma} \cdot \mathbf{n} dl \quad (11)$$

$$\bar{\mathbf{t}} = \frac{1}{L} \int_A \boldsymbol{\sigma} \cdot \mathbf{b}^+ dA \quad (12)$$

in which the stress tensor is that corresponding to the classical finite element approximation based on the continuous strain in Eq. (8). In general, the two equations do not coincide, as shown below for constant strain triangles with an embedded crack.

3.3. The constant strain triangular finite element

In this work, the simplest finite element has been selected. If a constant strain triangle with a strong discontinuity line (crack) is considered, such as that shown in Fig. 6a, and the positive normal pointing towards the solitary node is selected, then it can be shown that

$$\mathbf{b}^+ = \frac{1}{h} \mathbf{n}^+ \quad (13)$$

where h is the height of the triangle over the side opposite to the solitary node and \mathbf{n}^+ the unit normal to that side. With this, and the fact that the stresses are uniform, Eqs. (11) and (12) are reduced to

$$\bar{\mathbf{t}} = \boldsymbol{\sigma} \cdot \mathbf{n} \quad \text{for local equilibrium} \quad (14)$$

$$\bar{\mathbf{t}} = \frac{A}{hL} \boldsymbol{\sigma} \cdot \mathbf{n}^+ \quad \text{for global equilibrium} \quad (15)$$

where A is the area of the element and L the length of the crack. This shows that for local and global equilibrium to hold, it is required that $\mathbf{n}^+ = \mathbf{n}$ and $hL = A$. As a result of this, the following two conditions are imposed: (1) the discontinuity (crack) line being parallel to one of the sides of the triangle, and (2) the discontinuity line being located at mid height. Thus the potential crack lines satisfying both local and global equilibrium are those indicated by dashed lines in Fig. 6b.

In our approach the local equilibrium Eq. (14) is used in conjunction with the strain approximant (8). This leads to a non-symmetric formulation (SKON, according to Jirásek's nomenclature [49]). If Eq. (15) is imposed, then a symmetric formulation is obtained (Jirásek's KOS formulations [49]). Note, however, that both formulations tend to coincide when the crack runs parallel to one side of the element and at mid height (not through the centroid).

4. Numerical implementation

To simplify the computations, the bulk behaviour (material outside the crack) is assumed to be linear-elastic and anisotropic, although this approximation can be relaxed if necessary (e.g., [26]). The crack displacement vector \mathbf{w} is handled as two internal degrees of freedom which are solved at the level of the crack within the finite element (assumed to be a constant strain triangle).

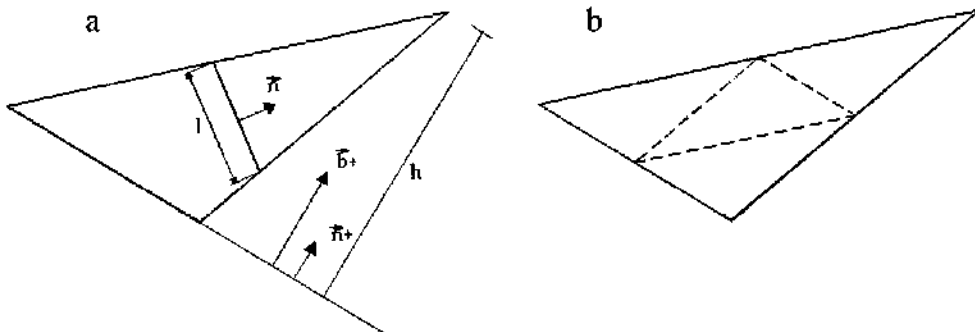


Fig. 6. Constant stress triangle: (a) geometrical definitions and (b) potential crack paths satisfying both global and local equilibrium (dashed lines).

4.1. Basic equations

One of the main tasks of the implementation is to compute the stress tensor in the element, which follows an algorithm similar to plasticity, since the stress tensor is given, from Eq. (8) and the hypothesis of elastic bulk material behaviour, as

$$\boldsymbol{\sigma} = \mathbf{E} : [\boldsymbol{\varepsilon}^a - (\mathbf{b}^+ \otimes \mathbf{w})^S] \quad (16)$$

where \mathbf{E} is the tensor of elastic moduli. Before computing the result of the stress, the crack displacement must be solved. The corresponding equation is obtained by substituting the foregoing expression for the stress into Eq. (14) and the result into the cohesive crack Eq. (2). The resulting condition is

$$\frac{f(\tilde{w})}{\tilde{w}} \mathbf{w} = [\mathbf{E} : \boldsymbol{\varepsilon}^a] \cdot \mathbf{n} - [\mathbf{E} : (\mathbf{b}^+ \otimes \mathbf{w})^S] \mathbf{n} \quad (17)$$

which can be rewritten as

$$\frac{f(\tilde{w})}{\tilde{w}} \mathbf{w} = [\mathbf{E} : \boldsymbol{\varepsilon}^a] \cdot \mathbf{n} - [\mathbf{n} \cdot \mathbf{E} \cdot \mathbf{b}^+] \mathbf{w} \quad (18)$$

or else

$$\left[\frac{f(\tilde{w})}{\tilde{w}} \mathbf{1} + \mathbf{n} \cdot \mathbf{E} \cdot \mathbf{b}^+ \right] \cdot \mathbf{w} = [\mathbf{E} : \boldsymbol{\varepsilon}^a] \cdot \mathbf{n} \quad (19)$$

where $\mathbf{1}$ is the second-order unit tensor. This equation is solved for \mathbf{w} using Newton Raphson's method given the nodal displacements (and so $\boldsymbol{\varepsilon}^a$) once the crack is formed and thus \mathbf{n} and \mathbf{b}^+ are also given. It is worth noting that \mathbf{E} and $f(\tilde{w})$ depend on the direction (angle γ).

One of the key points in the proposed method is how the crack is introduced in the element, i.e., how \mathbf{n} and \mathbf{b}^+ are determined.

4.2. Crack initiation

Initially, $\mathbf{w} = 0$ in the element, and \mathbf{n} and \mathbf{b}^+ are undefined. Thus, the element loads elastically and $\boldsymbol{\sigma} = \mathbf{E} : \boldsymbol{\varepsilon}^a$ until the tensile stress reaches tensile strength in a particular direction, as has been above exposed in Section 2.2. Then a crack is introduced perpendicular to the direction of the tensile stress that reached the tensile strength, and \mathbf{n} is computed as a unit eigenvector in the direction of γ .

Next, the solitary node and the vector \mathbf{b}^+ are determined by requiring the angle between \mathbf{n} and \mathbf{b}^+ to be the smallest possible (see Fig. 6). This is based on the fact that the tensor $\mathbf{n} \cdot \mathbf{E} \cdot \mathbf{b}^+$, and therefore the tangent stiffness matrix, is well conditioned when \mathbf{n} and \mathbf{b}^+ tend to be parallel. In this way, the pathological situations with $\mathbf{n} \cdot \mathbf{E} \cdot \mathbf{b}^+$ almost orthogonal are automatically avoided. For a constant strain triangle finite element, and given the direction of cracking, there are only three different modes of separating the nodes in two subelements. This is algorithmically achieved by looping over the three possible vectors \mathbf{b}^+ and looking for the one satisfying

$$\frac{|\mathbf{b}^+ \cdot \mathbf{n}|}{|\mathbf{b}^+|} = \max \quad (20)$$

4.3. Crack adaptation

The foregoing procedure is carried out at the element level, and is strictly local: no crack continuity is enforced or crack exclusion zone defined. This leads in many circumstances to locking after a certain crack growth. Such locking seems to be due to a bad prediction of the cracking direction in the element ahead of the pre-existing crack, as sketched in Fig. 7. To overcome this problem without introducing global algorithms (crack tracking and exclusion zones), we merely introduce a certain amount of crack adaptability within each element. The rationale behind the method is that the estimation of the principal directions in a triangular element is especially bad at crack initiation due to the high stress gradients in the crack tip zone where the new cracked element is usually located; after the crack grows further, the estimation of the principal stress directions ordinarily improves substantially. Therefore, we allow the crack to adapt itself to the later variations in principal stress direction while its opening is small. This crack adaptation is implemented very easily by stating that while the equivalent crack opening at any particular element is less than a threshold value \tilde{w}_{th} , the crack direction is recomputed at each step as if the crack were freshly created. After $\tilde{w} > \tilde{w}_{th}$, no further adaptation is allowed and the crack direction becomes fixed.

Threshold values must be related to the softening properties of the material, and values of the order of $0.1-0.2G_F/f_t$ are usually satisfactory. Here, G_F is the fracture energy and f_t the tensile strength. Until an in-depth parametric study is carried out, this is an orientative value to be taken as a starting point for analysis, since the dependence on the threshold may be dependent on the geometry and material properties. This simple expedient has proved to be extremely effective as shown in the examples presented next, and bears some resemblance with other approaches used to avoid crack locking.

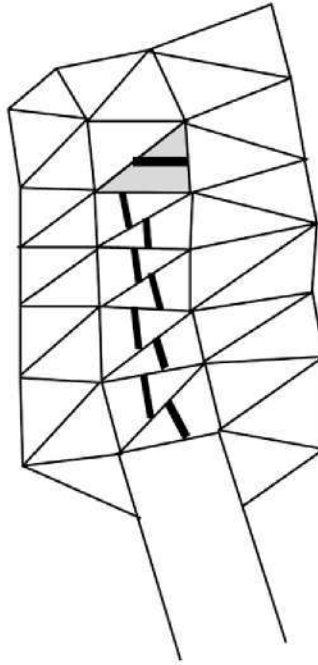


Fig. 7. Sketch of the crack locking: the prediction of cracking direction in the shaded element is wrong.

5. Overview of the experimental programme

5.1. Materials and specimens

To check the model, a series of mixed fracture tests were performed [61] on small masonry panels under TPB configuration with non-symmetric loading (Fig. 8). This test configuration has been successful for mixed-mode fracture of concrete and mortar [62,63].

This experimental programme is not intended to be a small-scale modelling of real masonry walls. The aim of using scaled specimens is to capture the essentials of the mixed-mode fracture of masonry while maintaining a reasonable experimental cost. This methodology, an alternative to full-scale testing, has been widely used in masonry research since the mid-1950s, and is helpful in understanding the interaction between bricks and mortar joints [22]. A scale factor of 1/4 was chosen, both to avoid difficulties in modelling the joint thickness, and to have a representative number of brick units in masonry specimens. Only geometric similitude requirements were considered, and the micro-mortar and the solid brick units used in this work were not intended to represent a real mortar, nor real brick units, as explained earlier.

Small-scale bricks of $48 \times 24 \times 10 \text{ mm}^3$ were cut from commercial solid clay bricks. Prismatic notched specimens of $240 \times 57.5 \times 37 \text{ mm}^3$, with a notch to depth ratio of 0.5, for fracture tests were sawn. See [26,61] for further details.

The mortar used for masonry was both designed to meet similitude requirements and assure a workable mix. It was composed of Portland cement CEM I 42.5 N (ASTM Type I) and siliceous sand of 1 mm maximum size, compatible with the scaled-down thickness of the joints of 3 mm. The grading of the sand complied with ASTM C-144 Standard. To improve the mechanical performance of the mortar, silica fume was added (13% of cement weight). Finally, superplasticiser was added to the mortar (3% of the cement and fume silica weight) to make the filling of the joints easier.

Prismatic specimens of $337.5 \times 75 \times 26.5 \text{ mm}^3$ were cast to characterise the mortar. Beams with a vertical joint between mortar and brick in the middle of the span were also cast to characterise the fracture and mechanical behaviour of the interface brick-mortar. Details may be also found in Refs. [26,61].

Masonry panels were manufactured with the mortar and the small-scale units described above. Panels with three orientations of the bed joints (0° , 45° and 90°) and size of $675 \times 150 \times 26.5 \text{ mm}^3$ were cast. The specimens were cast horizontally in prismatic ground steel moulds; small-scale bricks had been previously immersed in lime saturated water at 20°C for 24 h. Then, the bricks were carefully fixed in the mould and the fresh mortar was poured over the matrix of bricks. The thickness of the joints was 3 mm. The specimens remained in the moulds 48 h, covered with saturated sacking at room temperature. They were later taken to a curing room and left there at 20°C and 98% relative humidity until testing. The panels were notched in the middle of the span, with a notch to depth ratio of 0.5, before testing. In all cases the tip of the notch was inside a brick unit.

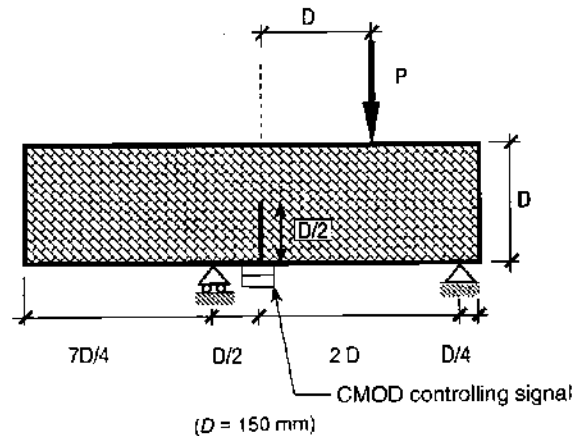


Fig. 8. Testing arrangement, geometry, dimensions, boundary conditions and instrumentation of the tested specimens under TPB configuration.

5.2. The characterisation tests

Characterisation fracture tests were performed on mortar, bricks and interface brick-mortar. Table 1 shows fracture energy and the tensile strength of them. Recommendations of RILEM 50-FMC [64] were adapted to these materials. See Refs. [26,61] for details.

The meso-scale approach was adopted for numerical modelling. As previously explained, this approach does not make any distinction between units and mortar, averaging the effect of the composite material through a fictitious continuous material. TPB fracture tests were performed following the RILEM 50-FMC [64] to obtain the fracture energy of the brickwork masonry for three orientations of the joints (0° , 45° and 90°). The values of the longitudinal deformation modulus and traction strength were indirectly obtained from this test. Table 2 summarises the results.

5.3. Mixed-mode fracture tests

The tests were carried out on the prismatic masonry panels described above, under TPB configuration. To induce mixed mode loading conditions, the test was performed under non-symmetric boundary conditions, as shown in Fig. 8. Twelve masonry panels of four orientations of the joints (0° , $\pm 45^\circ$ and 90°), were tested.

The masonry beams rested on two rigid steel cylinders laid on two ground supports, which allowed free rotation out of the plane of the beam and guarantee negligible friction rolling in the longitudinal direction of the beam. During the test, applied load, load-point displacement and CMOD were continuously recorded. The tests were performed in CMOD control, at a rate of 0.04 mm/min. Further details may be found elsewhere [26].

6. Numerical analysis of the mixed mode loading tests

The described model has been introduced in the commercial finite element program ABAQUS© [65] by means of a user subroutine for material (UMAT). An auxiliary external file containing the nodal coordinates and mesh connectivity is also used. This file would not be needed if the model were implemented as a user element, in a UEL subroutine. Nevertheless, the use of a UMAT subroutine avoids the formulation of the whole finite element (*v. gr.* shape functions) since this is automatically made by the program. No special difficulties were found in achieving a convergent solution. The independence of the finite element mesh (structured/unstructured and coarse/fine) was previously studied for the isotropic model [46].

The presented numerical procedure is used to reproduce the experimental results. Fig. 9 shows the deformed finite element meshes used to study the mixed-mode fracture of the brickwork masonry panels with the four orientations of the bed joints.

Table 1
Mechanical properties of the constituent elements of brick masonry.

Element	G_F (N/m)	f_t (MPa)
Brick	107	7.6
Mortar	86	7.6
Joint (brick-mortar)	10	-

Table 2

Mechanical properties of brick masonry under mode I fracture.

Orientation	G_F (N/m)	f_t (N/mm ²)	E (kN/mm ²)
Horizontal	75	5.8	28
45°	54	4.1	22
Vertical	33	2.4	21

Fig. 10 shows the experimental and the numerical prediction of the crack paths for the specimens with the four orientations of the bed joints. The numerical prediction is a sufficiently accurate approximation of the crack path. In this sense, it is noticeable that masonry exhibits a wider experimental scatter than other quasi-brittle materials such as mortar and concrete.

Figs. 11 and 12 compare the envelope of the experimental records load versus CMOD and load versus displacement of the application point of the load for specimens and different orientations of bed joints, with the numerical prediction.

7. Discussion

The numerical cohesive crack model proposed, based on the embedded strong discontinuity approach, accurately predicts the crack path and the experimental records load versus CMOD and displacement of the application point of the load for the specimens with different orientations of the bed joints. In contrast with previous works [24,27], based on the discrete crack approach, the proposed model supplies the advantage that does not require us to know the crack path for the implementation of the cohesive model. The model is an extension to anisotropic materials of the embedded cohesive crack model developed by the authors [45–47] for mixed-mode fracture of concrete and mortar (isotropic material).

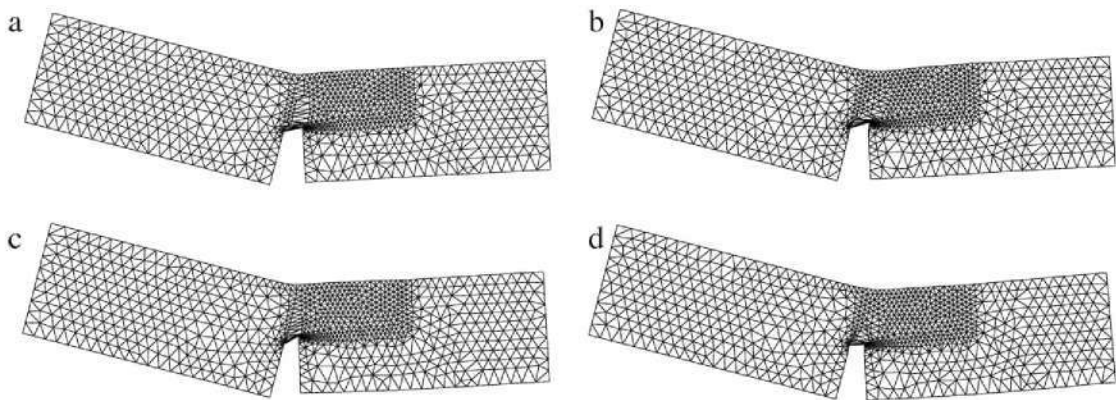


Fig. 9. Finite element deformed mesh for modelling the specimens with bed joints at: (a) 0°, (b) 45°, (c) 90°, and (d) -45°.

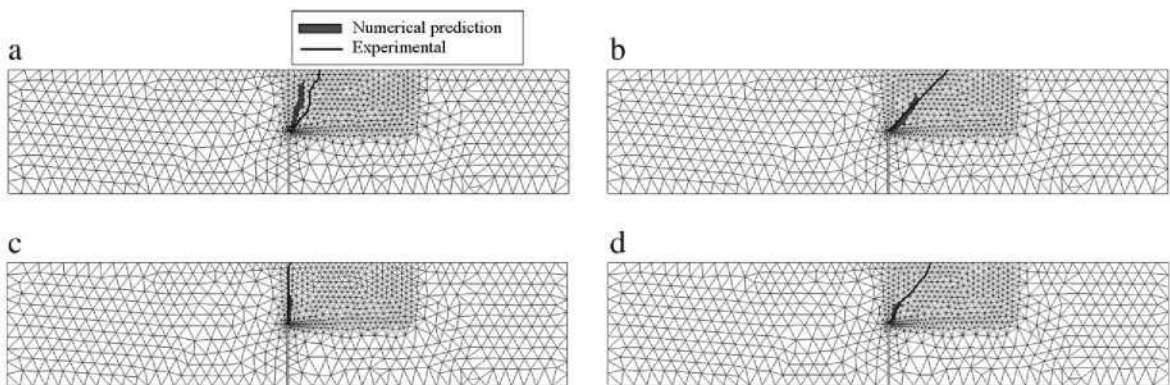


Fig. 10. Mean experimental (from three specimens) and numerical prediction of the crack path of the specimens with the bed joints at: (a) 0°, (b) 45°, (c) 90°, and (d) -45°.

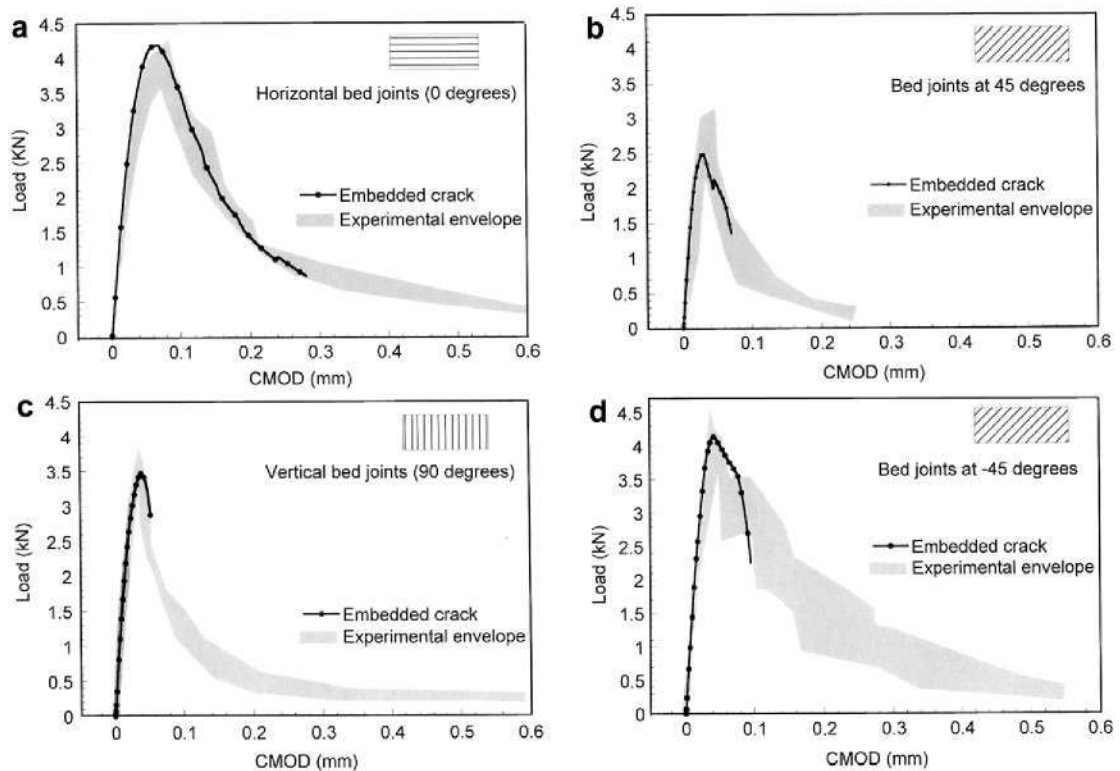


Fig. 11. Envelope of the experimental records and numerical prediction of load P versus CMOD for TPB specimens with the bed joints at: (a) 0° , (b) 45° , (c) 90° , and (d) -45° .

The model properly predicts the peak load of the experimental records (see Figs. 11 and 12). Nevertheless, since the masonry is more brittle than concrete or mortar, the descending branch of the experimental records of load versus CMOD and displacement of the application point of the load is not simulated until the end of the curve. The model simulates the complete curve of the concrete and mortar tests [45,47]. These problems of convergence are more marked with the most brittle specimens of brick masonry, specimens with bed joints at 45° and 90° , in which the experimental descending branch of the curve is more vertical and even shows snap-back. But in all cases, the peak load and significant part of the descending branch is properly predicted, enough for engineering purposes.

From the experimental point of view, the interface brick-mortar was shown as the weakest part of the masonry. The highest failure load was reached on the specimens whose orientation of the brick layers was so that the crack cut bricks and joints. The lowest failure load was reached when the crack run by the interface brick-mortar (see Refs. [26,27,61] for details). This experimental behaviour is clearly reproduced by the numerical model.

It is worth noting that the parameters needed by the proposed model are measured by means of standardized tests, different of the simulated tests, and the prediction is reached without any kind of fitting or tuning procedure. The experimental work adopted for the model checking is not intended to be small-scale testing. Further more work must be carried out to extend this modelling to full-scale masonry structures.

8. Final remarks and conclusions

A numerical model, based on the embedded strong discontinuities approach, is proposed to model the mixed-mode fracture of masonry and quasi-brittle anisotropic materials. As in previous works [45–47], based on this approach, the deformation is localised on a line using the concept of the cohesive crack, and the discrete constitutive relation for mixed-mode fracture is a cohesive crack with a central-force model. The model extends previous works [45–48,50,51] to an anisotropic material, the masonry, and it avoids crack tracking [52,60] or exclusion zones for crack growing.

A triangular constant strain finite element is formulated and implemented in the commercial standard code ABAQUS© [65]. The algorithm used to obtain the crack displacement vector can be formulated at the crack level and therefore the static condensation of the stiffness matrix at the element level is avoided. The choice of the solitary node is made in a way that leads to the automatic propagation of the crack without tracking algorithm or exclusion zones. The stress locking effects are solved by letting the embedded crack in the finite element to adapt itself to the stress field while the crack opening does

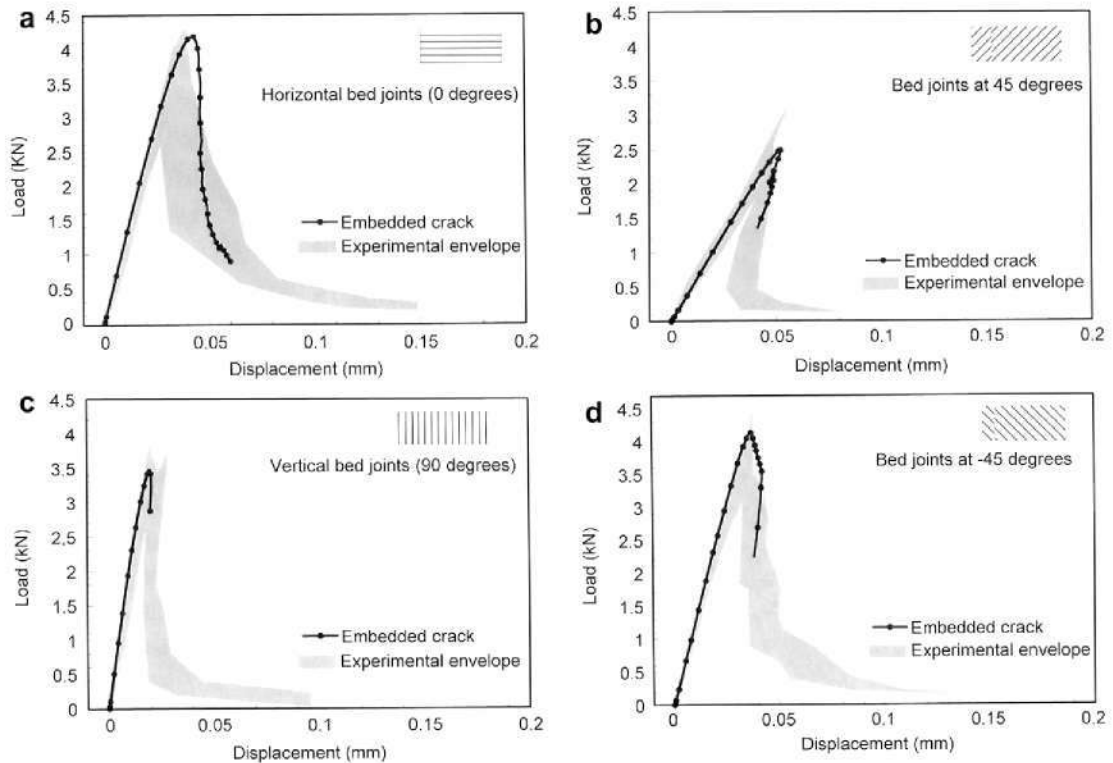


Fig. 12. Envelope of the experimental records and numerical prediction of load P versus load point displacement for TPB specimens with the bed joints at: (a) 0° , (b) 45° , (c) 90° , and (d) -45° .

not exceed a small threshold value. A generalised Rankine criterion is adopted to take into account the anisotropy of the quasi-brittle materials.

A series of mixed-mode fracture tests on small masonry panels, with different inclinations of the bed joints, under non-symmetric TPB, were adopted for checking the model. The objective was not to be a small-scale modelling of real masonry walls. Extension of these results to full-scale masonry structures requires additional work. The numerical model correctly predicts the experimental results.

The proposed model procedure reaches a balance between accuracy and simplicity, and provides a helpful tool in predicting the fracture of large masonry structural elements when a single macro-crack, or finite number of them, is the main failure mechanism. The presented model does not include distributed cracking or damage in the structure and applies in the case of a macro-crack occurring, but this approximation can be relaxed if necessary [26].

The presented numerical model and the experimental results emphasise that the cohesive crack models, taking into account the anisotropy of the masonry, are promising tools in the simulation of the mixed-mode fracture of the masonry in large structural elements. For engineering purposes, the averaging of the masonry properties provides sufficiently precise data for cohesive modelling. For small masonry elements, a more detailed analysis of fracture micro-mechanisms, especially interface brick-mortar interaction, is required.

The numerical simulations show that the foregoing combination of simple ingredients leads to a method in which the cohesive crack automatically propagates without the need for a tracking algorithm or exclusion zones. Hence, the embedded cohesive crack approach turns out to be yet an effective and simpler alternative to other more sophisticated methods for the simulation of concrete damage and fracture.

Acknowledgements

The authors gratefully acknowledge the financial support for the research provided by the Spanish Ministerio de Ciencia e Innovación under Grants BIA-2005-09250-CO3-02 and BIA-2008-03523. In addition, they also thank the Ministerio de Fomento under Grant MFOM-01/07 for the complementary financial support received.

References

- [1] Steward MG, Lawrence S. Structural reliability of masonry walls in flexure. *Masonry Int* 2002;15(2):48–52.
- [2] Grimm CT. Masonry cracks: a review of literature. *Masonry: materials, design, construction and maintenance*. In: Harris HA, editor. ASTM STP 992. Philadelphia: American Society for Testing and Materials; 1988. p. 257–80.

- [3] Naraine K, Sinha S. Stress-strain for brick masonry in biaxial compression. *ASCE J Struct Eng* 1992;118(6):1451-61.
- [4] Alshabani M, Sinha S. Stress-strain characteristics of brick masonry under uniaxial cyclic loading. *ASCE J Struct Eng* 1999;125(6):600-4.
- [5] Khalaf FM, Hendry AW, Fairbairn DR. Study of the compressive strength of blockwork masonry. *ACI Struct J* 1994;91(4):367-75.
- [6] Riddington JR, Naom NF. Finite element prediction of masonry compressive strength. *Comput Struct* 1994;52(1):113-9.
- [7] Lourenço PJ. Computational strategies for masonry structures. PhD thesis, Delft, The Netherlands; 1996.
- [8] Lourenço PJ, Rots J, Blaauwendraad J. Continuum model for masonry: parameter estimation and validation. *ASCE J Struct Eng* 1998;124(6):642-52.
- [9] Bernardini A, Modena C, Valluzzi MR. Load transfer mechanisms in masonry: friction along a crack within a brick. *Mater Struct* 1998;31:42-8.
- [10] Anhoine A. Derivation of the in-plane elastic characteristics of masonry through homogenization theory. *Int J Solids Struct* 1995;32(2):137-63.
- [11] Mojsilovic N, Marti P. Strength of masonry subjected to combined actions. *ACI Struct J* 1997;94(6):633-42.
- [12] Jukes P, Riddington JR. The failure of brick triplet test specimens. *Masonry Int* 2001;15(1):30-3.
- [13] Bosiljkov V, Zarnic R, Kralj B, Pande GN. Experimentally-based computational modelling of masonry. In: Pande GN, Middleton J, Kraj B, editors. *Computer methods in structural Masonry-4*. New York: E&FN Spon; 1998. p. 103-10.
- [14] Page AW. Finite element model for masonry. *ASCE J Struct Div* 1978;104(8):1267-85.
- [15] Abdou L, Saada RM, Meftah F, Mebarki A. Experimental investigations of the joint-mortar behavior. *Mechanics* 2006;33:370-84.
- [16] Abdou BE, Hamid AA, Harris HG. Flexural behavior of reinforced concrete masonry walls under out of plane monotonic loads. *ACI Struct J* 1996;93(3):327-35.
- [17] van der Pluijm R. Out of plane bending of masonry behaviour and strength. PhD thesis, Delft, The Netherlands; 1999.
- [18] Fathy AM, Planas J, Sancho JM. A numerical study of masonry cracks. *Eng Fail Anal*; in press. 10.1016/j.engfailanal.2008.02.011.
- [19] Corneau AF, Shrive NG. Development of a fracture mechanics approach for masonry. In: Bailly ME, Spodler DE, editors. *7th North American Masonry Conference*; 1996. p. 379-88.
- [20] Corneau AF, Shrive N. Fracture Mechanics and future strength design of masonry. In: Bailly ME, Spodler DE, editors. *7th North American Masonry Conference*; 1996. p. 477-88.
- [21] Carpinteri A, Chiaia B, Bocca P. Size dependence of strength and fracture properties of brickwork masonry walls. *ASCE J Engng Mech* 1997;123(8):816-22.
- [22] Guinea GV, Hussein G, Elices M, Planas J. Micromechanical modelling of brick-masonry fracture. *Cem Concr Res* 2000;30:731-7.
- [23] Alfaiate J, Almeida JR. Discrete cracking of masonry walls. In: *European congress on computational methods in applied sciences and engineering. ECCOMAS; 2000*, 15 p.
- [24] Galvez JC, Reyes E, Casati MJ. Brickwork masonry failure under tensile/shear loading. *Masonry Int* 2000;9:184-91.
- [25] Reyes E, Casati MJ, Galvez JC. Normal/shear cracking of brickwork masonry. In: Li V et al., editors. *Fracture mechanics of concrete structures*; 2004. p. 415-22.
- [26] Reyes E. Fracture of the brickwork masonry under tensile/shear loading. PhD thesis [in Spanish], Spain: Ciudad Real; 2004.
- [27] Reyes E, Casati MJ, Galvez JC. Cohesive crack model for mixed mode fracture of brick masonry. *Int J Fract* 2008;151:29-55.
- [28] van der Pluijm R. Non-linear behavior of masonry under tension. *HERON* 1997;42(1):25-53.
- [29] Page AW. The strength of brick masonry under biaxial tension-compression. *Int J Masonry Constr* 1983;3:26-31.
- [30] Rots JG. Numerical simulation of cracking in structural masonry. *Heron* 1991;36:49-63.
- [31] Dhanasekar M, Kleeman P, Page AW. Biaxial stress-strain relations for brick masonry. *J Struct Engng ASCE* 1985;3(5):1085-100.
- [32] Papa E, Nappi A. Numerical modeling of masonry: a material model accounting for damage defects and plastic strains. *Appl Math Model* 1997;319-35.
- [33] Lourenço PB, Rots J. On the use of micromodels for the analysis of masonry shear walls. In: Pande, Middleton, editors. *Computer methods in structural Masonry-2*, Swansea; 1993. p. 14-26.
- [34] Zucchini A, Lorenço PB. A micro-mechanical model for the homogenization of masonry. *Int J Solids Struct* 2002;39:3233-55.
- [35] Salerno G, Bilotta A, Porco F. A finite element with micro-scale effects for the linear analysis of masonry brickwork. *Comput Methods Appl Mech Eng* 2001;190:4365-78.
- [36] Rahman MA, Anand SC. Empirical Mohr-Coulomb failure criterion for concrete block-mortar joints. *J Struct Engng ASCE* 1994;120:2408-22.
- [37] Lourenço PB, Ramos L. Characterization of cyclic behavior of dry masonry joints. *J Struct Engng ASCE* 2004;130:779-86.
- [38] Cecchi A, Di Marco R. Homogenized strategy toward constitutive identification of masonry. *J Engng Mech ASCE* 2002;128:688-97.
- [39] Uva G, Salerno G. Towards a multiscale analysis of periodic masonry brickwork: a FEM algorithm with damage and friction. *Int J Solids Struct* 2006;43:3739-69.
- [40] Milani G, Lourenço PB, Tralli A. Homogenised limit analysis of masonry walls, Part I: failure surfaces. *Comput Struct* 2006;84:166-80.
- [41] Papa E. A unilateral damage model for masonry based on homogenization procedure. *Mech Cohes - Frict Mater* 1996;1:349-66.
- [42] Pietruszczak S, Ushaksaraei R. Description of inelastic behavior of structural masonry. *Int J Solids Struct* 2003;40:4003-19.
- [43] Massart TJ, Peerlings RHJ, Geers MGD, Gottscheiner S. Mesoscopic modeling of failure in brick masonry accounting for three-dimensional effects. *Engng Fract Mech* 2005;72:1238-53.
- [44] Giambanco G, Rizzo S, Spallino R. Numerical analysis of masonry structures via interface models. *Comput Methods Appl Mech Eng* 2001;190:6493-511.
- [45] Sancho JM, Planas J, Fathy AM, Gálvez JC, Cendón DA. Three-dimensional simulation of concrete fracture using embedded crack elements without enforcing crack path continuity. *Int J Numer Anal Methods Geomech* 2007;31:173-87.
- [46] Sancho JM, Planas J, Cendón DA, Reyes E, Gálvez JC. An embedded crack model for finite element analysis of concrete fracture. *Eng Fract Mech* 2007;74:75-86.
- [47] Sancho JM, Planas J, Gálvez JC, Reyes E, Cendón DA. An embedded cohesive crack model for finite element analysis of mixed mode fracture of concrete. *Fatigue Fract Engng Mater Struct* 2006;29:1056-65.
- [48] Simo J, Oliver J, Armero F. An analysis of strong discontinuities induced by strain softening in rate-independent inelastic solids. *Comput Mech* 1993;12:277-96.
- [49] Jirásek M. Comparative study on finite elements with embedded cracks. *Comput Methods Appl Mech Eng* 2000;188:307-30.
- [50] Jirásek M, Belytschko T. Computational resolution of strong discontinuities. In: Mang, Rammeerstorfer, Eberhardsteiner editors. *Fifth World Congress on Computational Mechanics*, Vienna, Austria; 2002.
- [51] Simo J, Rifai S. A class mixed assumed strain methods and the method of incompatible modes. *Int J Numer Methods Eng* 1990;29:1595-638.
- [52] Oliver J, Huespe A, Samaniego E, Chaves EWV. On strategies for tracking strong discontinuities in computational failure mechanics. In: *Fifth World Congress on Computational Mechanics*, Vienna, Austria; 2002.
- [53] Hillerborg A, Modeer M, Petersson P. Analysis of crack formation and crack growth in concrete by means of fracture mechanics and finite elements. *Cem Concr Res* 1976;6:773-82.
- [54] Dugdale DS. Yielding of steel sheets containing slits. *J Mech Phys Solids* 1960;8:100-4.
- [55] Barenblatt G. The mathematical theory of equilibrium cracks in brittle fracture. *Adv Appl Mech* 1962;7:55-129.
- [56] Cendón DA, Gálvez JC, Elices M, Planas J. Modelling the fracture of concrete under mixed loading. *Int J Fract* 2000;103:293-310.
- [57] Bažant ZP, Planas J. Fracture and size effect in concrete and other quasibrittle materials. New York: CRC Press; 1998.
- [58] Galvez JC, Cendón DA, Planas J. Influence of shear parameters on mixed-mode fracture of concrete. *Int J Fract* 2002;118:163-89.
- [59] Bocca P, Carpinteri A, Valente V. Fracture analysis of brick masonry: size effects and snap-back analysis. *Mater Struct* 1989;27:99-105.
- [60] Oliver J. Modelling strong discontinuities in solid mechanics via strain softening constitutive equations. Part 1: fundamentals. Part 2: numerical simulations. *Int J Numer Methods Engng* 1996;39:3575-623.

- [61] Reyes E, Casati JM, Galvez JC. Experimental scale model study of cracking in brick masonry under tensile and shear stress. *Mater Construct* 2008;58:69–83.
- [62] Gálvez JC, Cervenka J, Cendón DA, Saouma V. A discrete crack approach to normal/shear cracking of concrete. *Cem Concr Res* 2002;32:1567–85.
- [63] Gálvez JC, Elices M, Guinea GV, Planas J. Mixed mode fracture under proportional and non-proportional loading. *Int J Fract* 1998;94:267–84.
- [64] RILEM 50-FMC Committee Fracture Mechanics of Concrete. Determination of the fracture energy of mortar and concrete by means of three-point bend tests on notched beams, *Materiaux et Constr* 1986;18:285–290.
- [65] ABAQUS (2003). Standard user's manual, Version 6.3, Rhode Island, USA.